Influence of local convective heat flux on solidification, contraction and wall detachment behavior of molded chocolate during air cooling

Author(s):
Grob, Lucas; Papadea, Konstantina; Braun, Peter; Windhab, Erich J.

Publication date:
2021-03

Permanent link:
https://doi.org/10.3929/ethz-b-000467399

Originally published in:
Innovative Food Science & Emerging Technologies 68, https://doi.org/10.1016/j.ifset.2021.102629

Innovative Food Science and Emerging Technologies 68 (2021) 102629

Contents lists available at ScienceDirect

Innovative Food Science and Emerging Technologies

journal homepage: www.elsevier.com/locate/ifset

Influence of local convective heat flux on solidification, contraction and wall detachment behavior of molded chocolate during air cooling

Lucas Grob *, Konstantina Papadea, Peter Braun, Erich J. Windhab

ETH Zurich, Institute of Food, Nutrition and Health, Schmelzbergstrasse 9, 8092 Zurich, Switzerland

ARTICLE INFO

Keywords:
Convective heat transfer
Heat transfer coefficient
Cooling
Confectionery

ABSTRACT

The cooling process is an important step during chocolate production. It influences final product quality characteristics such as gloss, texture and melting behavior. Furthermore, it is a high energy consuming operation and its optimization leads to an increase in energy efficiency of the chocolate production. Dark chocolate was cooled in a pilot-scale cooling tunnel with cooling air temperatures of $T_{air} = 2$, 12 and 18 °C and air mean velocities of $v_{in} = 1.5$, 3.5, and 6.0 m s^{-1}. Convective heat transfer coefficients at the top and the bottom of the mold were received from model calculations applying a CFD model. Crystallization and detachment behavior from the mold walls were newly analyzed by measuring the damping characteristics of ultrasound waves transferring the filled molds during cooling. In addition, for this-like treated well-tempered dark chocolate, the crystallization and detachment behavior were analyzed in further detail. The convective heat transfer from the bottom of the mold increases in flow direction due to the existence of a typical mold geometry-dependent recirculating zone of the cooling air below the chocolate mold and also dependent on the local air velocity. It was shown that depending on intensity and homogeneity of the heat transfer in the air-cooling phase, the structure density of the chocolate can be increased which has a positive impact on resulting product quality characteristics. Moreover, the detachment of the chocolate from the mold wall was demonstrated to have an optimum for typical chocolate plate formats with 125 g weight at an apparent heat flux of 550 W/m^2, for which the time until detachment reaches a minimum.

1. Introduction

Convective cooling is an important unit operation, frequently applied in food processing and requiring a substantial amount of energy. The optimization of such high energy consuming processes is crucial to make food production more sustainable and energy efficient. At the same time, food products of premium sensory and nutritious quality are requested in order to achieve a high level of consumer acceptance. An intrinsic requirement for many premium quality food products is their homogeneity which in turn requires their homogeneous treatment during manufacture. Accordingly, for chocolate/chocolate confectionery homogeneous cooling conditions at optimized cooling rates decide about a homogeneous distribution of structural characteristics like uniform fat polymorph crystallization and related product surface gloss and melting characteristics. Consequently, within the present work we identified correlations between spatial and temporal temperature inhomogeneities appearing during cooling and related solidification of chocolate and the appearance of cooling spots and fat bloom. Measures to prevent inhomogeneities and surface errors focused on the cooling conditions with special regard on the homogeneity of the "cooling history" in all spatial zones of the finished product (Loeser, 2017; Minifie, 1989).

Prior to cooling and solidification upon crystallization, chocolate is pre-crystallized (= tempered) in order to generate a small fraction (ca. ≤ 1 vol%) of the cocoa butter fat crystal nuclei in the polymorphic forms β_V or β_{VI}. Around such crystal nuclei the remaining cocoa butter crystallizes during cooling according to the pre-crystallized polymorphic pattern (Windhab, 2008). A controlled pre-crystallization of the chocolate mass is crucial since only the right fat crystal polymorph structure leads to sufficient product contraction and consequently enables easy demolding of the chocolate from the mold (Metin & Hartel, 2005; Svanberg, Ahrné, Lorén, & Windhab, 2013, 2011). Furthermore, cooling process conditions such as contact time, temperature and relative humidity of the cooling air impact on chocolate crystallization and on its adhesion to the mold surface and thus as well on the ease of demolding. During the chocolate cooling process, both the latent heat generated

* Corresponding author.
E-mail address: lugrob@ethz.ch (L. Grob).

https://doi.org/10.1016/j.ifset.2021.102629
Received 8 September 2020; Received in revised form 22 January 2021; Accepted 23 January 2021
Available online 29 January 2021

Table 1
Chocolate composition.

Ingredients	Original [wt%]	Final [wt%]
Sugar	50.87	47.85
Cocoa butter	7.36	38.96
Cocoa mass	41.38	12.77
Lecithin	0.42	0.40
Vanilin	0.02	0.02
Total fat content	**30.45**	**34.50**

during crystallization, as well as the specific heat to cool the product to a desired temperature have to be removed in the cooling tunnel. The latent heat of dark chocolate is 46 J/g and the specific heat is 1.59 J/(g K) (Clegg, 2001). Therefore to cool down 1 g of chocolate from typically 30 °C molding temperature, to 12 °C demolding temperature in a cooling tunnel, requires heat energy removal of 29 J, which results in a total of 75 J to cool down and crystallize 1 g of chocolate. The heat is removed both by conduction through solid materials (chocolate and mold) and by forced convection of the cooling air flow (Tewkesbury, Stapley, & Fryer, 2000), whereas radiation plays a minor role in cooling tunnels for molded chocolate confectionery (Beckett, 2008). The determination of convective heat transfer coefficients α_{conv} [W/(m^2 K)] is therefore essential for optimization of the chocolate cooling process. Convective heat transfer coefficients α_{conv} depend on various cooling air properties, density, specific heat, viscosity, thermal conductivity and its velocity. Further, it is also dependent on the geometry and surface roughness of the solid object in contact with the cooling air (Singh & Heldman, 2014). The aim of this study was to link the total convective heat flux also to the resulting techno-functional material properties such as its internal temperature field, contraction behavior, and resulting detachment. Thus, first Finite Element Method (FEM) based simulations were conducted and compared with heat flux sensor based measurements to optimally derive convective heat transfer coefficients on the bottom and top of the mold. To further connect this to the structure development in the chocolate product, ultrasonic attenuation measurements during cooling, crystallization/solidification and detachment of chocolate from the mold were recorded and high resolution camera images taken from the product surface.

2. Materials and methods

2.1. Sample preparation

Dark chocolate (Max Felchlin AG, Schwyz, Switzerland) with 30.45 wt% cocoa butter fraction and pure prime pressed cocoa butter (Olam Cocoa B.V., Netherlands) were used for the cooling experiments. Both the chocolate as well as the cocoa butter were molten at 55 °C under partial vacuum (p_v = 200 mbar) during ≥12 h to fully melt the entire material and to remove incorporated air. Cocoa butter was added to the chocolate to ensure a final fat content of 34.50 wt%. The final sample composition is given in Table 1.

The sample was cooled to 31.3 ± 0.5 °C in a stainless steel tempering beaker with a diameter of 130 mm to prevent re-melting of the subsequently added seed crystals. To ensure homogeneous cooling, it was stirred at 120 ± 10 rpm by a four-blade impeller with a diameter of 100 mm. The cooled sample was pre-crystallized by seeding with cocoa butter crystal suspension (CBCS) with a crystal concentration of ≈13 wt % (Padar, Jeelani, & Windhab, 2008). The CBCS was produced by a single-stage crystallizer SeedMaster Cryst (Bühler AG, Uzwil, Switzerland (Windhab & Zeng, 1999)). The pre-crystallized sample was stirred at 500 ± 10 rpm during 2 min to homogeneously disperse the crystals within the entire sample. A total sample mass of ≈ 250 g was used. The final crystal concentration related to the total fat content in the sample was 0.5 wt%, equivalent to a temper index of TI ≈ 6.

2.2. Pilot-scale cooling tunnel

A custom-made pilot-scale cooling tunnel (ETH Zurich, Switzerland) was used for the chocolate cooling experiments as well as for the convective heat transfer measurements. The measuring cell within the cooling tunnel had a cross section of 500 × 200 mm. The mold was positioned on top of 4 × 4 mm in diameter rods in the center of the measuring cell at a height of 100 mm with the cooling air flow in parallel to the mold surface (Fig. 1a)). Further, to ensure a fully developed flow the mold was placed at a distance of 6 x D_h of 1.7 m from the bend. Chocolate cooling experiments were conducted at three different air temperatures of T_{air} = 2, 12 and 18 °C. The cooling tunnel was PID controlled and regulated by the injection and evaporation of liquid nitrogen and an electrical heating coil. Further, three different air velocities of v_{air} = 1.5, 3.5 and 6 m s^{-1} were set. All trials were conducted, after 20 min of stable temperature conditions, in triplicate (N = 3). A

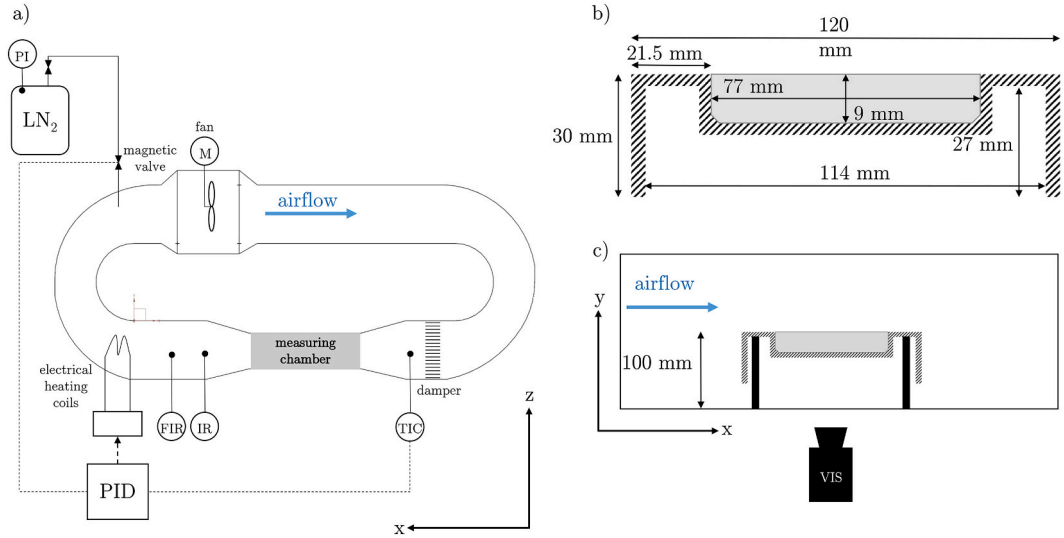

Fig. 1. Cooling tunnel setup: a) Schematic illustration of the pilot-scale cooling tunnel. b) Dimensions of single polycarbonate mold placed in the measuring chamber.

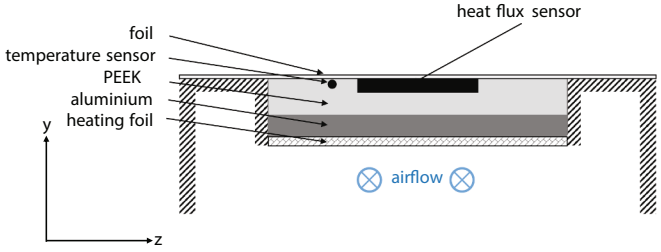

Fig. 2. Measurement setup for heat flux sensor. Side view of the different layers. From top to bottom: self-adhesive foil, PEEK plate with included heat flux sensor and temperature sensor, aluminum plate, and heating foil.

video camera (Powershot S5SI, Tokyo, Japan) was set up at a distance of 200 mm below the mold. The camera was placed outside of the cooling tunnel to avoid disturbance of the air flow. The entire mold detachment process was recorded through a transparent acrylic glass window.

2.3. Molding

Single polycarbonate molds (Max Riner AG, Rupperswil, Switzerland) were used for the chocolate cooling experiments as well as for the convective heat transfer measurements (Fig. 1b)). The molds had a dimension of 220x120x30 mm to produce chocolate bars with a flat surface and a chocolate plate product dimension of 159x77x9 mm. The 30 mm high mold edge (H) formed a cavity at the bottom of the mold (Fig. 1 b). The cavity had a length of $L_{cav} = 114$ mm and a height of $H_{cav} = 18$ mm. The mold bottom intruded into the cavity and had a length of $L_{int} = 77$ mm and a height of $H_{int} = 9$ mm. The pre-heated polycarbonate molds (heating cabinet set to 32 °C) were filled with 120 ± 5 g of the pre-crystallized chocolate and placed in the center of the measuring chamber of the cooling tunnel (Fig. 1a).

2.4. Detachment analysis

The detachment of the chocolate from the mold wall was calculated as a function of the total area from the video data by MATLAB (see Supplementary material). The times to reach a detached area of 50 and 75% were taken for comparison.

2.5. Heat flux sensor

A silicone gSKIN-XO heat flux sensor (greenTEG, Zurich, Switzerland) was used to deter-mine the local convection heat transfer coefficients at the top and bottom of the chocolate mold. The sensor had a dimension of 30x30x2 mm and a relative measurement error of ±3% and was placed in the middle of the mold cavity at a length coordinate of l = 60 mm. The sensor was calibrated according to ISO 8301. The polycarbonate mold used for the chocolate cooling experiments, was reamed to fit the heat flux measurement setup consisting of various layers. A heating foil acted as a chocolate substitute and ensured a constant heat source heated by a power of 10 W. The heating foil was placed underneath an aluminum plate of 10 mm thickness, which ensured homogeneous heat distribution. The aluminum plate was placed on top of a 10 mm thick polyether ether ketone (PEEK) plate (Kundert AG, Jona, Switzerland) that was reamed to fit the heat flux sensor. To obtain an even surface ensuring unaffected air flow, a 0.01 mm thick self-adhesive foil covered the entire surface. The influence of the foil can be neglected since it has minimal thickness and surface roughness similar to the mold material (Fig. 2).

The heat flux sensor consisted of multiple connected thermocouples, defined as thermopiles (Kaviany & Kanury, 2002). Due to the temperature difference between the two surfaces of the sensor, a heat flux q and therefore a measurable electrical output voltage U is generated. The heat flux $\dot{q}_{tot}$ is proportional to the output voltage U. This is based on the Seebeck effect. The thermocouples were connected in series increasing the output voltage U to be in a measurable range.

The convective heat transfer coefficient α_{conv} was calculated using Newton's law for cooling. Both the cooling air temperature T_{air}, measured before the mold, as well as the surface temperature of the sensor T_S were measured by glass-encapsulated NTC thermistors (Epcos, Germany). The surface temperature T_S was measured on the reamed surface of the PEEK plate, 3 mm next to the sensor to prevent interference with the heat flux measurement. Since the thermal conductivity of PEEK is almost identical to the thermal conductivity of the heat flux sensor ($k_{PEEK} = 0.82$ W m^{-1} K^{-1} ≈ $k_S = 0.80$ W m^{-1} K^{-1}), it is assumed that the required surface temperature of the sensor T_S is the same as the measured surface temperature of the PEEK plate. The total heat flux $\dot{q}_{tot}$ was determined by the measured sensor output voltage U and the temperature-corrected sensor sensitivity S:

$$\dot{q}_{tot} = \frac{U}{S} \tag{1}$$

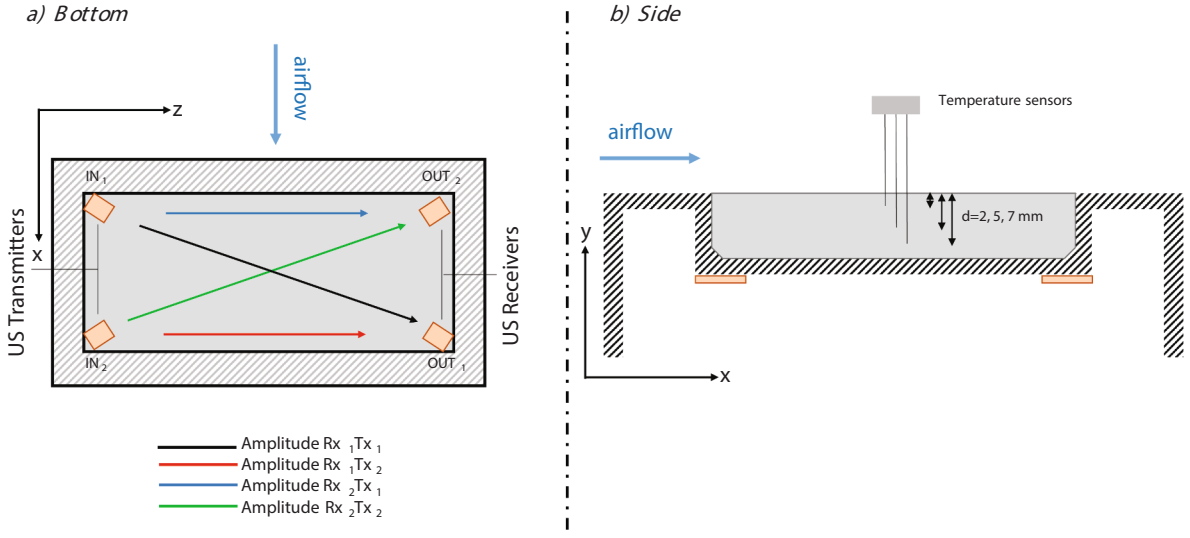

Fig. 3. Mold setup: a) Setup of 4 ultrasonic transducers at the bottom of a mold, 2× IN and 2× Out; b) 1 temperature sensors from top immersed in the chocolate.

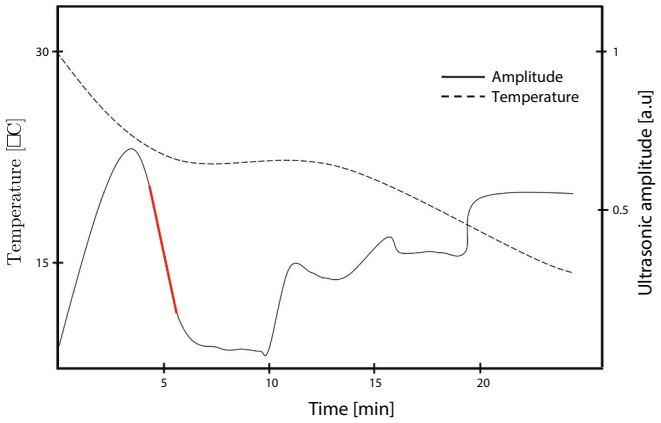

Fig. 4. Schematic evolution of the ultrasound amplitude and temperature during the cooling process for a mold filled with tempered chocolate. The dashed line indicates the product temperature at the center of the chocolate during the cooling process. Red line indicates the rate of ultrasonic attenuation increase during the crystallization of the chocolate. Adapted from (Grob et al., 2021).

Both the sensor output voltage U as well as both temperatures T_{air} and T_S were measured every second and logged by a DaqPRO 5300 (Fourier Technologies Ltd., RoshHa'ayin, Israel) device during 1 min after an adjustment period of 14 min to reach steady-state conditions.

$$\dot{q}_{conv} = \dot{q}_{tot} - \dot{q}_{rad} = \alpha_{conv} \cdot (T_s - T_{air}) \quad (2)$$

The convective heat flux $\dot{q}_{conv}$ is obtained by correcting the total heat flux $\dot{q}_{tot}$ by the radiation heat flux $\dot{q}_{rad}$, with the latter calculated by $\dot{q}_{rad} = \varepsilon \cdot \sigma \cdot (T_S^4 - T_{air}^4)$ including the Boltzmann constant $\sigma = 5.67 \cdot 10^{-8}$ $Wm^{-2}K^{-4}$ and the emissivity of the surface $\varepsilon = 0.725$ (Çengel & Ghajar, 2007). All experiments were conducted in triplicates ($N = 3$).

2.6. Ultrasonic attenuation

Four 10–100 kHz broadband piezoelectric patch transducers DuraAct TMP-876.SP1 (PI, Ceramic, Lederhose, Germany) with a dimension of 16 × 13 × 0.5 mm were attached by a double-sided adhesive tape to the corners at the bottom of the mold (see Fig. 3). Two transmitted pulsed Gaussian-windowed, 5-fold sinusoidal waves (IN_1, IN_2) and the other two acted as receivers (OUT_1, OUT_2). The resulting amplitude pathways are denoted as RxTx with the corresponding number of the receiver and transmitter.

Fig. 4 schematically shows the evolution of the US amplitude (solid line) during the cooling of chocolate. The dashed line accordingly is the corresponding temperature in the center of the chocolate. The rate of ultrasonic attenuation increase (= US damping gradient), mainly caused by the crystallization triggered increase in chocolate viscosity, was defined as the slope of the linearized US amplitude decrease per time during the initial fat crystallization upon cooling according to Grob, Papadea, Braun, & Windhab, 2021. This segment is represented by the red line in Fig. 4.

2.7. Modeling

Cooling air flow and heat flux simulations were performed by Ansys 17.2 CFX. The model mold dimensions were used as described in Fig. 1 b). The cooling tunnel height was set at 200 mm, the considered cooling channel section length was 500 mm. The model mold was positioned at 50 mm from the air inlet in the middle of the cooling tunnel. Design and meshing were carried out with Designmodeler and Meshdesigner. A mesh study was carried out to make the simulations perform satisfyingly accurate. The air flow calculations were based on the SST turbulence model. SST calculates the free air stream flow with a kε-model and the wall boundary layer with a kω-model. Inflow conditions were set at a normal speed of 1.5, 3.5, and 6.0 m s^{-1}, 12 °C and at a turbulence intensity of 10%. The outlet condition was set at an average static pressure of 0 Pa. The cooling air properties, such as specific heat capacity, dynamic viscosity and thermal conductivity were taken from thermodynamic tables for dry air (Engineering-Toolbox, 2019). The wall temperature of the mold was set constant at 31 °C. All simulations were tested for mesh independence with a minimum size of 9 10^{-5} m and maximum size of 5 10^{-4} m, performed with double precision and a converged solution with a residual mean square error of 10^{-6} was reached.

2.8. Statistical analysis

To estimate the goodness of prediction between measured and calculated local heat transfer coefficient values the relative root mean square error (RRMSE) was calculated according to Eq. 3.

$$RRMSE = \frac{\sqrt{\frac{1}{N}\sum_{i=1}^{N}\left(\alpha_{meas,i} - \alpha_{calc,i}\right)^2}}{\frac{1}{N}\sum_{i=1}^{N}\alpha_{calc,i}} \quad (3)$$

Where i is the target number and $N = 3$. Further the detachment behavior was analyzed using the one-way Analysis of Variance (ANOVA) with Tukey HSD post hoc test computed with IBM SPSS Statistics 24. Multiple comparisons between all pair-wise means was performed. A p-value less than 0.05 was considered statistically significant.

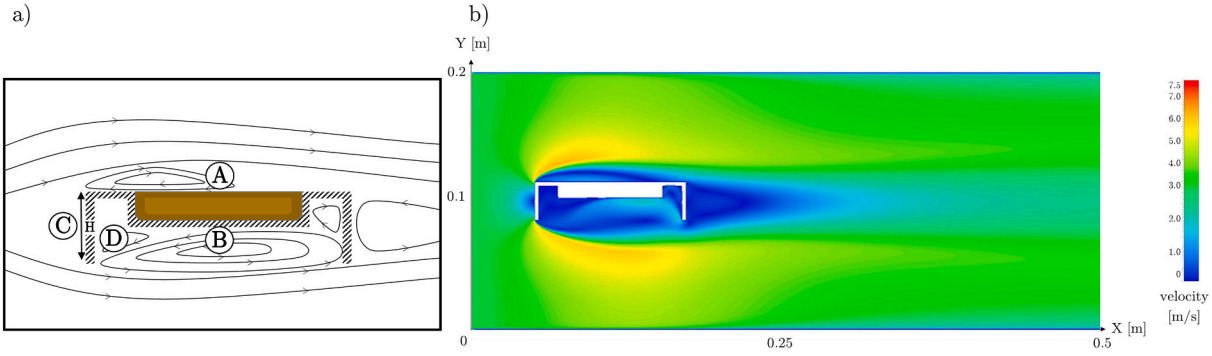

Fig. 5. Model mold. a) Schematic drawing of the velocity field around a chocolate mold. A: on top of the mold, B: at the bottom of the mold, C: at the leading edge with height H, and D: in wake region created by the cavity. b) Computed air flow velocity field around a model mold with H = 30 mm edge height for an inflow air velocity of $v_{in} = 3.5$ m s^{-1} and with a cooling air temperature of $T_{air} = 12$ °C.

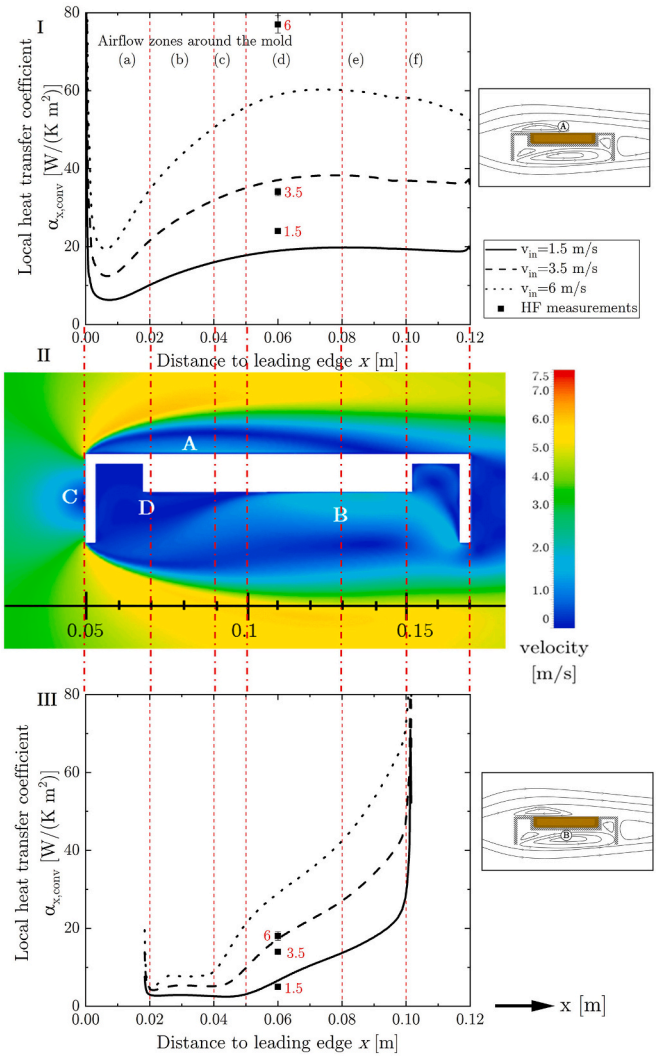

Fig. 6. Comparison of simulation-based computed local heat transfer coefficients $\alpha_{x,conv}$ cooling air velocity fields along top (I) and bottom (III) of surfaces of a model mold with 30 mm edge height, at cooling air temperature of $T_{air} = 12$ °C and constant initial mold surface temperature of $T_s = 31$ °C. Black squares indicate measurements at corresponding air velocities (indicated in red numbers) with the heat flux sensor.

3. Results and discussion

3.1. Heat transfer coefficients around the mold

When air of different temperature flows past a body, the resulting convective heat transfer is directly coupled to the flow pattern. Depending on the shape of the body, the local flow pattern will evolve differently (Fig. 5 a). On top of the mold (A), the air is first deflected from the leading edge (C) with a height H before the tuft reattaches to the surface and establishes a parallel flow layer situation. Due to the leading edge geometry a cavity is formed, at the bottom of the mold (B) and wake regions (D) are created were the air barely moves. Fig. 5 b) depicts a FEM simulation result for the model mold exposed to an initial air velocity $v_{in} = 3.5$ m s^{-1} and a cooling air temperature of $T_{air} = 12$ °C. With the addition of a constant initial mold surface temperature of 31 °C the local heat transfer coefficients $\alpha_{x,conv}$ could be extracted and they are plotted as a function of the distance to the leading edge in Fig. 6.

Fig. 6 depicts the local heat transfer coefficient along the top (I) and at the bottom (III) surfaces of the model mold with H = 30 mm edge height. Focusing on the development of the flow on top (Fig. 6, I), a steady increase of the heat transfer coefficient is observed. A local minimum is located close to the leading edge. In this zone reduced air velocities and a recirculation zone are derived from the simulated velocity field (Fig. 6, II). Further downstream, the mold top surface flow develops and forms a laminar sublayer. There the simulation-derived local heat transfer coefficient $\alpha_{x,conv}$ approaches an approximately constant value. It must be noted that the leading edge height H and the resulting tuft length due to the air velocity play a major role in the observed local heat transfer coefficient. Ota & Kon, 1974 showed in their work similar behavior for the local heat transfer coefficient with distance to the leading edge. Moreover, a maximum heat transfer coefficient was found at a distance to leading edge ratio of x/H = 8. At the mold bottom surface (Fig. 6, III), where a wake region with low velocities is observed right behind the inflow edge plate, $\alpha_{x,conv}$ has lowest values (< 10 Wm^{-2} K^{-1}). Further downstream, the mold bottom surface the air velocity and with it the local convective heat transfer coefficient increase steeply since the downstream mold bottom edge guides cooling air backwards in a jet-like flow pattern which has a pronounced vertical component. This suppresses the development of a laminar flow boundary layer and thus supports convective heat transfer efficiently as demonstrated in Fig. 6, particularly in flow zone (e) but still relevant in zone (d). According to Larchevêque, Sagaut, Mary, Labbé, and Comte (2003), the cavities at the mold bottom are shallow since their length/height ratio L/H > 1, in the experimentally investigated case L/H ≈ 6. The simulation results were compared to measurements of the local heat transfer coefficient in the center of the top and bottom surfaces mold. This-like measured $\alpha_{x,conv}$ values are indicated in Fig. 6 (square shaped point with red numbers indicating the inflow air velocity in m s^{-1}). Further Fig. 7 explicitly compares the calculated and measured heat transfer coefficients $\alpha_{x,conv}$ in the center of the top and the bottom mold surface for the different air velocities. The calculated heat transfer coefficient was averaged along the length of the heat flux sensor (30 mm). At the lower inflow air velocities simulated and measured values agree well. At the highest air velocity of 6 m s^{-1} the model simulation over predicts the heat transfer coefficients at the mold bottom surface center and under predicts at the mold top surface center. The over and under prediction might be to lower and higher turbulence occurring in the setup at different velocities which is not reflected in the model. Thus, the calculated relative root mean square error (RRMSE) with 33% is relatively large.

3.2. Process dependent contraction and detachment behavior

Cooling conditions, such as temperature and air velocity, affect the crystallization temperature. The slower the chocolate is cooled, the higher the temperature at which latent heat evolves and the larger the amount of latent heat (Tewkesbury et al., 2000). Fast cooling enables nucleation and growth of unstable polymorphs at the expense of the β_V polymorph form, causing a rapid increase in viscosity and limiting molecular diffusion and further crystal growth (Rejman, 2017). In addition to heat transfer through convection (chocolate to cooling air)) and conduction (chocolate to mold), there is also internal heat conduction within the chocolate that limits heat transfer (Biot-Number > 1 (Tewkesbury et al., 2000)). Consequently, strong cooling conditions are not equally effective for the product center and for its surface layer (Ehlers, 2012). To take into account changes in air velocity and temperature, an apparent integral heat flux $\dot{q}_{app}$ is calculated:

$$\dot{q}_{app} = \overline{\alpha}_{conv} \cdot \left(T_{choc,t=0} - T_{air}\right) \quad (4)$$

The related averaged heat transfer coefficient $\overline{\alpha}_{conv}$ at the mold bottom surface as derived from the simulation based model calculations was exemplary taken with the initial chocolate temperature $T_{choc,t=0}$ set to 31 °C. To further include a structural parameter which determines the product quality characteristics, the fat crystal network formation was considered according to (Birkhofer, 2007), by amplitude damping

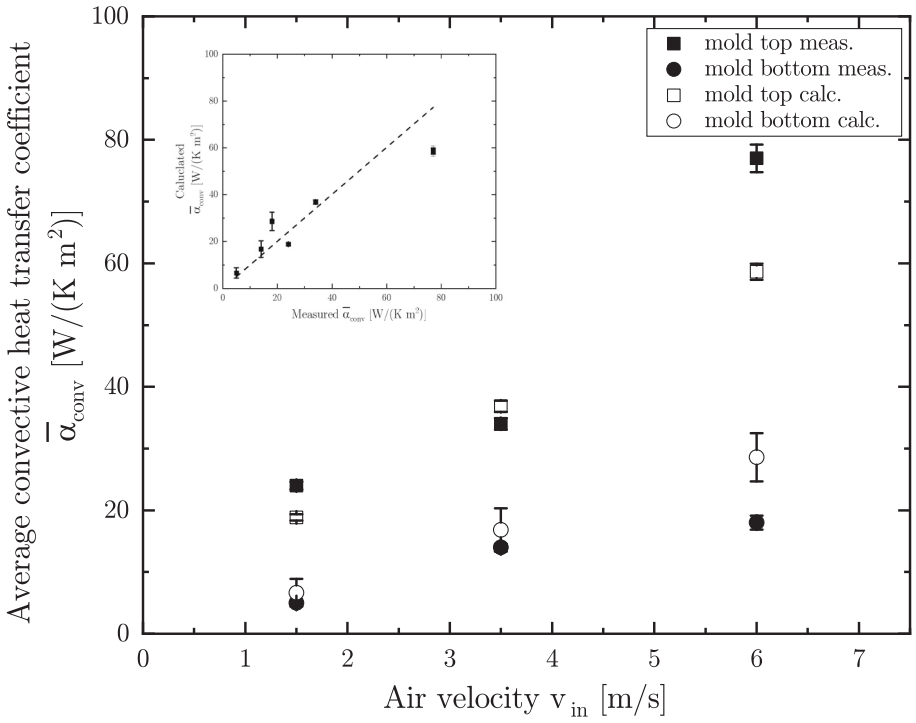

Fig. 7. Calculated and measured average convective heat transfer coefficients for the length of the sensor (30 mm) on top and bottom of the mold as a function of air velocity v_{in}.

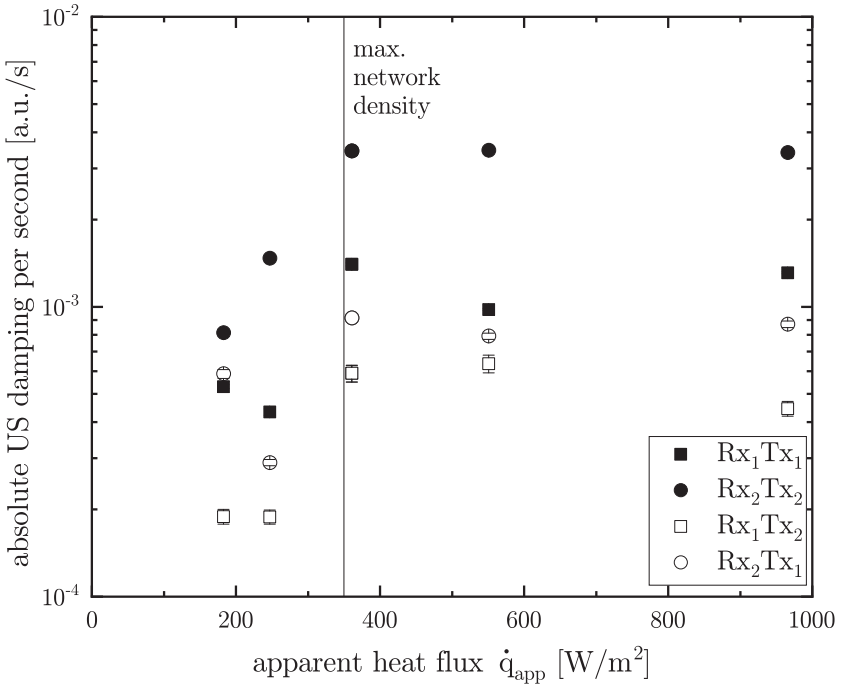

Fig. 8. US damping gradient during the cooling/crystallization phase of chocolate before entering into the solidification dominated structure formation (crystal network formation) phase for different apparent heat flux applied at the bottom of the mold.

detection of ultrasonic (US) waves passing through the crystallizing chocolate mass during the cooling process. Evaluating the increase in US damping as a function of cooling time made us define the US wave amplitude decrease per second (=US damping gradient) as a crystal structure development indicator during cooling of the chocolate in the mold before solidification started. Such measured heat flux dependency of the US damping gradient is shown in Fig. 8. The higher the heat flux the higher the absolute US damping gradient. Low heat fluxes below 350 W/m^2 showed almost no damping, towards higher heat flux a plateau was reached.

US attenuation when passing a multiphase fluid system is determined by multiple factors, such as temperature, scattering, and visco-inertial dissipation losses. When damping increases all these factors contribute synchronously. The higher the absolute US damping gradient the higher

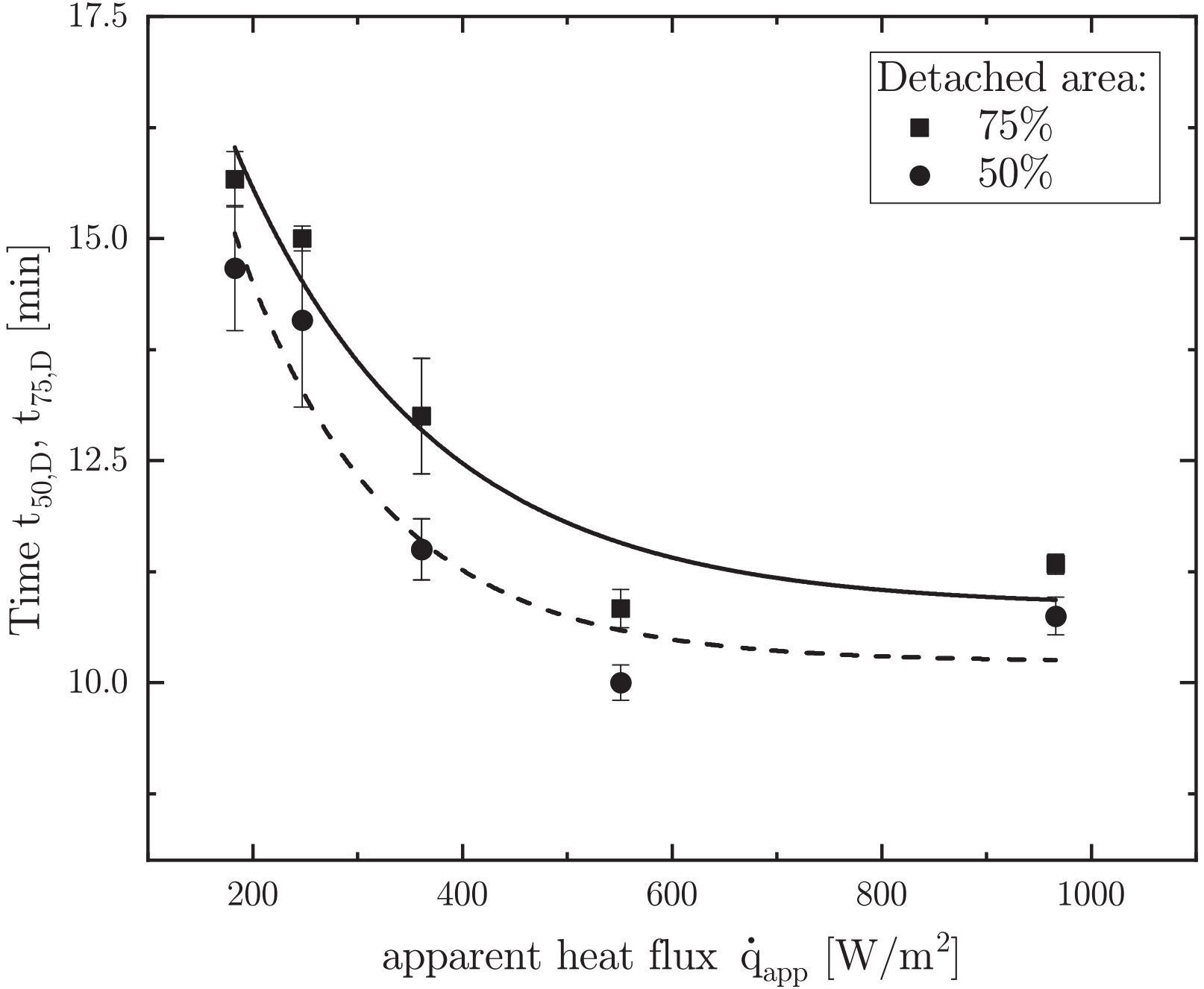

Fig. 9. Time to reach 50% and 75% detachment during the contraction phase of chocolate for different apparent heat flux applied at the bottom of the mold. Line indicates exponential decay fit of the data ($y = y_0 + A\, e^{-x/t}$). For 50%: $y_0 = 10.85$, $A = 13.75$, and $t = 186.85$ at $R^2_{adj} = 0.89$. For 75%: $y_0 = 10.23$, $A = 17.67$, and $t = 140.81$ at $R^2_{adj} = 0.86$.

the chocolate structure density increase due to accelerated fat crystal formation and related viscosity increase (Ehlers, 2012). When the transient temperature curve, measured within the chocolate shows an inflection point, crystallization rate is at the maximum (Ehlers, Hanselmann, & Windhab, 2013). Thus, the US damping gradient reaches its maximum simultaneously. During this cooling phase the chocolate still fully adheres to the mold surface. With ongoing crystallization/crystal network formation and chocolate solidification the elasticity (solid body characteristics) of the chocolate increases and a contraction effect gets superimposed due to the higher density of stable polymorph cocoa butter fat crystals compared to the liquid cocoa butter melt. This leads to the build-up of tensile- and shear stresses within the chocolate product in the mold resulting in a detachment from the mold wall. Thereby, the amount of chocolate surface attached to the mold's wall decreases with time. To evaluate and compare the mold surface detachment kinetics, the detachment times at which 50% and 75% of the surface area are detached ($t_{50,D}$, $t_{75,D}$) were taken. Fig. 9 demonstrates $t_{50,D}$ and $t_{75,D}$ as a function of the apparent (integral) heat flux (see eq.4). The one-way ANOVA test (see Supporting materials) revealed, at low apparent heat flux <250 W/m^2 the detachment time $t_{50,D}$ and $t_{75,D}$ does not significantly differ ($p > 0.05$). An approximate time shift of ca. 37 s between $t_{50,D}$ and $t_{75,D}$ could be estimated under the chosen experimental conditions. However, the fitted exponential decay curves can only be a rough approximation since the mold detachment rarely proceeds steadily but stepwise due to the stresses which build up in the chocolate sample during solidification and contraction and which relax by a stepwise moving front of the detached area.

This is also demonstrated in Fig. 4 by the stepwise reduction of the US wave amplitude damping during the detachment phase. For heat fluxes ≥ ca. 550 W/m^2 no further decrease in detachment time was detected ($p > 0.05$). When larger apparent heat fluxes were applied for lowest cooling air temperatures investigated ($T_{air} = 2$ °C) at a cooling air velocity of $v_{in} = 3.5$ m s^{-1}, the detachment time increased again (Fig. 9; ca. 950 W/m^2 apparent heat flux). We hypothesize that this is caused by some tendentiously less stable polymorph fat crystal formation and related decrease in maximum product contraction capability.

4. Conclusion

Coupling measuring and numerical model simulation methodologies for the quantification of local and integral heat fluxes from a crystallizing chocolate melt in a mold to a surrounding cooling air flow in a cooling tunnel under industrially relevant conditions, could be successfully demonstrated. Moreover, resulting heat transfer information was coupled with the complex, transient (i) temperature development in the crystallizing, latent heat generating chocolate mass and (ii) the crystal network structure development in the sample. The latter was shown to be sensitively detectable by a custom-made ultrasound (US) wave amplitude damping in-line measuring technology (Detachlog; (Windhab, Mehrle, & Pfister, 2009)). The applied CFD model simulation of a cooled, chocolate filled model mold within a cooling tunnel was compared to measurements using heat flux sensors. The model-based simulations successfully predicted the local heat transfer coefficient on the top and bottom surfaces of the mold. A derived integral apparent heat flux correlated with the observed, quantified crystallization and detachment behavior of the chocolate. The detachment behavior was in-line measured via a camera system applying transparent mold material and correlated with the US attenuation measurements. Revealing that the attenuation reached a plateau at an apparent (integral) heat flux of 350 Wm^{-2} where the fat crystal network reached its maximal density and viscosity before entering into the solidification phase. For heat flux ≥ ca. 550 Wm^{-2}, the detachment was not further accelerated. In view of the maximum network density and the time to detachment suggest that the process time can be minimized without impeding the quality when the boundary condition of the apparent heat flux of ca. 400 Wm^{-2} is kept. Thus, the temperature, during a time optimized cooling of chocolate with 6 m s^{-1}, is best set around 15 °C.

Declaration of Competing Interest

The authors have no conflict of interest to be declared.

Acknowledgements

This work was supported by Innosuisse [Project number 18839.1 PFEN-LS], Switzerland. We would like to thank Bruno Pfister and Jan Corsano for technical support. Especially for modeling questions Daniel Meier has to be mentioned. Further for his support with the "Detach-Log", we would like to thank Josquin Rosset, ZHAW School of Engineering.

Appendix A. Supplementary data

Supplementary data to this article can be found online at https://doi.org/10.1016/j.ifset.2021.102629.

References

Beckett, S. T. (Ed.). (2008). *Industrial chocolate manufacture and use*. Oxford, UK: Wiley-Blackwell. https://doi.org/10.1002/9781444301588.

Birkhofer, B. H. (2007). *Ultrasonic in-line characterization of suspensions*. ETH Zürich. https://doi.org/10.3929/ethz-a-005457848

Çengel, Y. A., & Ghajar, A. J. (2007). *Heat and mass transfer: Fundamentals and applications* (4th ed.). Boston: McGraw-Hill.

Clegg, S. (2001). *Thermal conductivity of chocolate*.

Ehlers, D. (2012). *Controlled crystallization of complex confectionery fats*. ETH Zürich. https://doi.org/10.3929/ethz-a-009922089

Ehlers, D., Hanselmann, W., & Windhab, E. J. (2013). Online Tempercurve analysis of praline products with the objective of cooling process optimization. *Journal of Food Process Engineering, 36*, 292–301. https://doi.org/10.1111/j.1745-4530.2012.00691.x

Engineering-Toolbox. (2019). Dry air properties. https://www.engineeringtoolbox.com/dry-air-properties-d_973.html.

Grob, L., Papadea, K., Braun, P., & Windhab, E. J. (2021). In-line detection method for crystallization, contraction and mold detachment during cooling of confectionery products. *Journal of Food Engineering, 292*, 110322. https://doi.org/10.1016/j.jfoodeng.2020.110322

Kaviany, M., & Kanury, A. (2002). Principles of heat transfer. *Applied Mechanics Reviews, 55*, B100–B102. https://doi.org/10.1115/1.1497490

Larchevêque, L., Sagaut, P., Mary, I., Labbé, O., & Comte, P. (2003). Large-eddy simulation of a compressible flow past a deep cavity. *Physics of Fluids, 15*, 193–210. https://doi.org/10.1063/1.1522379

Loeser, U. (2017). *Instrumentation, in: Beckett's industrial chocolate manufacture and use* (pp. 555–597). John Wiley & Sons, Ltd. https://doi.org/10.1002/9781118923597.ch24

Metin, S., & Hartel, R. W. (2005). *Crystallization of fats and oils, in: Bailey's industrial oil and fat products*. Hoboken, NJ, USA: John Wiley & Sons, Inc.. https://doi.org/10.1002/047167849X.bio021

Minifie, B. W. (1989). *Chocolate, cocoa and confectionery: Science and technology* (3rd ed.). Springer US.

Ota, T., & Kon, N. (1974). Heat transfer in the separated and reattached flow on a blunt flat plate. *Journal of Heat Transfer, 96*, 459–462. https://doi.org/10.1115/1.3450227

Padar, S., Jeelani, S. A. K., & Windhab, E. J. (2008). Crystallization kinetics of cocoa fat systems: Experiments and modeling. *Journal of the American Oil Chemists' Society, 85*, 1115–1126. https://doi.org/10.1007/s11746-008-1312-0

Rejman, L. L. S. (2017). *Premium chocolate through cooling process optimization – An in-line monitoring approach*. ETH Zürich. https://doi.org/10.3929/ethz-b-000217342

Singh, R. P., & Heldman, D. R. (2014). Introduction to food engineering. In *Food science and technology international series* (Fifth edit.). Amsterdam: Elsevier, Academic Press.

Svanberg, L., Ahrné, L., Lorén, N., & Windhab, E. (2011). Effect of pre-crystallization process and solid particle addition on microstructure in chocolate model systems. *Food Research International, 44*, 1339–1350. https://doi.org/10.1016/j.foodres.2011.01.018

Svanberg, L., Ahrné, L., Lorén, N., & Windhab, E. (2013). Impact of pre-crystallization process on structure and product properties in dark chocolate. *Journal of Food Engineering, 114*, 90–98. https://doi.org/10.1016/j.jfoodeng.2012.06.016

Tewkesbury, H., Stapley, A. G., & Fryer, P. (2000). Modelling temperature distributions in cooling chocolate moulds. *Chemical Engineering Science, 55*, 3123–3132. https://doi.org/10.1016/S0009-2509(99)00578-3

Windhab, E. J. (2008). Tempering. In S. T. Beckett (Ed.), *Industrial chocolate manufacture and use*. Oxford, UK: Wiley-Blackwell. https://doi.org/10.1002/9781444301588.

Windhab, E. J., Mehrle, Y., & Pfister, B. (2009). *Method for the in-line measurement of the setting, contraction and wall release behaviour of confectionery/chocolate products which have been poured into moulds during production, and apparatus for carrying out this method.* WO2009138246A1.

Windhab, E. J., & Zeng, Y. (1999). *Method of producing seed crystal suspensions based on melted fat.* WO002000072695A1.